Laser-synthesized TiN nanoparticles for biomedical applications: Evaluation of safety, biodistribution and pharmacokinetics

Ivan Zelepukin, Anton Popov, Victoria Shipunova, Gleb Tikhonowski, Aziz Mirkasymov, Elena Popova-Kuznetsova, Sergey Klimentov, Andrei Kabashin, Sergey Deyev

Laser-synthesized TiN nanoparticles for biomedical applications: evaluation of safety, biodistribution and pharmacokinetics

Ivan V. Zelepukin[a,b,c #], Anton A. Popov[a #], Victoria O. Shipunova[a,b,c], Gleb V. Tikhonowski[a], Aziz B. Mirkasymov[a,b], Elena A. Popova-Kuznetsova[a], Sergey M. Klimentov[a], Andrei V. Kabashin[a,d] *, Sergey M. Deyev[a,b,e,f] *

[a]*MEPhI, Institute of Engineering Physics for Biomedicine (PhysBio), Moscow, Russia;* [b]*Shemyakin-Ovchinnikov Institute of Bioorganic Chemistry of Russian Academy of Sciences, Moscow, Russia;* [c] *Moscow Institute of Physics and Technology, Dolgoprudny, Russia;* [d] *Aix-Marseille University, CNRS, LP3, Marseille, France;* [e] *Sechenov University, Center of Biomedical Engineering, Moscow, Russia;* [f] *Tomsk Polytechnic University, Research Centrum for Oncotheranostics, Tomsk, Russia.*

[#] These authors contributed equally to this work

Corresponding author E-mail: kabashin@lp3.univ-mrs.fr, biomem@mail.ru

Abstract

Having plasmonic absorption within the biological transparency window, titanium nitride (TiN) nanoparticles (NPs) can potentially outperform gold counterparts in phototheranostic applications, but characteristics of available TiN NPs are still far from required parameters. Recently emerged laser-ablative synthesis opens up opportunities to match these parameters as it makes possible the production of ultrapure low size-dispersed spherical TiN NPs, capable of generating a strong phototherapy effect under 750-800 nm excitation. This study presents the first assessment of toxicity, biodistribution and pharmacokinetics of laser-synthesized TiN NPs. Tests in vitro using 8 cell lines from different tissues evidenced safety of both as-synthesized and PEG-coated NPs (TiN-PEG NPs). After systemic administration in mice, they mainly accumulated in liver and spleen, but did not cause any sign of toxicity or organ damage up to concentration of 6 mg kg^{-1}, which was confirmed by the invariability of blood biochemical parameters, weight and

hemotoxicity examination. The NPs demonstrated efficient passive accumulation in EMT6/P mammary tumor, while concentration of TiN-PEG NPs was 2.2-fold higher due to “stealth” effect yielding 7-times longer circulation in blood. The obtained results evidence high safety of laser-synthesized TiN NPs for biological systems, which promises a major advancement of phototheranostic modalities on their basis.

Keywords: titanium nitride (TiN) nanoparticles; pulsed laser ablation in liquids (PLAL); biodistribution; pharmacokinetics; toxicity

1. Introduction

Plasmonic nanoparticles (NPs) present one of most promising classes of advanced nanomaterials for nanomedicine and nano-bioengineering [1,2]. Capable of generating collective oscillations of free electrons (plasmons) under optical excitation, these NPs exhibit a strong absorption band in optical spectra with the absorption cross-section exceeding that of conventional absorbing dyes by many orders of magnitude [3]. For many noble metal NPs, such an absorption band takes place in the UV and visible range [3,4], which opens up avenues for the implementation of photonic imaging and therapeutic modalities. First of all, this is photothermal therapy (PTT) [5–7], which profits from a selective conversion of light stimuli into heat by nanomaterials accumulated in the tumor area. Such heat nanosources can locally kill cancer cells and stimulate anti-tumor immune response of the organism [8]. It is important that the PTT can be easily combined with photoacoustic imaging modalities [9,10] to visualize tumor area and monitor the therapeutic outcome. Owing to chemical stability and a good biocompatibility [11], gold (Au) NPs look the most suitable for these applications, but since spherical Au NPs have their absorption band (520-540 nm) outside the biological transparency window (630-900 nm), one has to engineer more complex core-shell [5,9] or nanorod [3,6] nanostructures

in order to shift the absorption peak toward this window. However, these structures are usually very large (e.g., the size of core shells having the plasmonic feature in the IR is in the range of 100-200 nm), which drastically complicates their excretion from the organism [12] and can cause toxic effects associated with a residual accumulation, while the nanorods require stabilization by non-biocompatible cetyltrimethylammonium bromide [6], can have difficulties for excretion from the body, and under some conditions loose their IR plasmonic properties as a result of shape modification during photothermal procedures [13,14].

Titanium nitride (TiN) NPs are now actively discussed as an alternative plasmonic material for biomedical applications [15,16]. As follows from theoretical studies [17,18], TiN NPs can have a red-shifted peak around 650-800 nm, which makes it a promising candidate for photonic therapy and imaging. The feasibility of using TiN NPs as contrast agents in photoacoustic imaging and sensitizers of photothermia of cancer has already been confirmed and tested in biological systems [15,19]. However, biological applications *in vivo* are very demanding to parameters of nanomaterials and typically require uniform size and shape of NPs, high biocompatibility in the absence of any contamination by toxic by-products, low visibility by the immune system, easy clearance, etc [1]. Such requirements are not easy to satisfy using conventional synthesis pathways. Indeed, TiN NPs prepared by wet chemistry methods are often contaminated by hazardous substances [20,21], which strongly limits their prospects. On the other hand, being prepared by alternative dry methods (e.g., a direct nitridation of TiO_2 powders [22] or plasma assisted processing [19,23]) and dispersed in aqueous solutions, TiN NPs typically present widely size-dispersed nanostructures of irregular shape (cigar-like, ellipsoidal) in partially aggregated state [19,23], which complicates their stabilization in

solutions (even after coating with polymers), delivery *in vivo* and clearance from the body.

We recently reported the synthesis of a novel type of titanium nitride nanoparticles, which demonstrate much advantageous characteristics for biomedical applications [24]. Our method of synthesis was based on femtosecond laser-induced ablation from a solid target immersed in a liquid ambient (deionized water, acetone) to produce nanoclusters, which then cool down and coalesce to form a colloidal NPs solution [25–27]. Laser-synthesized TiN NPs had ideal spherical shape and low size-dispersion under a controllable mean size (between 3-4 nm and several tens of nm), while solutions of bare (ligand-free) NPs demonstrated excellent stability due to a strong negative charge of NPs leading to the electrostatic repulsion effect [24]. Profiting from a strong plasmonic peak centered between 650 and 700 nm with significant tail over 800 nm, we evidenced a strong photothermal effect and demonstrated its successful application for the treatment of cancer cells [24]. These first data give a promise for a major advancement of cancer treatment modalities based on unique properties of laser-synthesized TiN NPs, but the potential of this new material has yet to be confirmed by results of its biological assessment.

This study is conceived as the first attempt to evaluate the interaction of laser-synthesized titanium nitride NPs, namely as synthesized bare NPs (TiN NPs) and polyethylene glycol (PEG)-coated NPs (TiN-PEG NPs), with biological systems. Using *in vitro* assessment and *in vivo* evaluation in a mouse model, toxicity, biodistribution and pharmacokinetics of these NPs are studied. Based on the obtained results, it was concluded that both types of laser-synthesized NPs present safe objects, while TiN-PEG NPs can offer a longer circulation in the bloodstream and a better passive accumulation in tumors. Combined with the capability of providing a strong photothermal effect, laser-

synthesized TiN NPs look like a novel nanomaterial promising a major advancement of nanomedicine-based cancer treatment modalities.

2. Materials and Methods

2.1 Materials

A hot-pressed target for laser ablative synthesis was purchased from GoodFellow (Cambridge, UK). Chemicals were obtained from the following suppliers. Sigma-Aldrich (USA): 3-(4,5-Dimethyl-2-thiazolyl)-2,5-diphenyl-2H-tetrazolium bromide (MTT), propidium iodide, RNAse A, nitric acid, ammonium hydroxide, ethylenediaminetetraacetic acid (EDTA), dimethyl sulfoxide (DMSO); Alfa Aesar (USA): bovine serum albumin (BSA); Nanocs Inc. (USA): mPEG-Silane (2000 Da); Virbac (France): Zoletil; Bioveta (Czech Republic): Rometar; Sintez (Russia): heparin; Biolegend (USA): rat anti-mouse RBC antibody TER-119; Jackson ImmunoResearch (USA): goat anti-rat antibody; HyClone (USA): Dulbecco's Modified Eagle's Medium (DMEM), fetal bovine serum (FBS); PanEko (Russia): L-glutamine, penicillin/streptomycin.

2.2 Synthesis of TiN Nanoparticles

TiN NPs were synthesized by the technique of femtosecond (fs) laser ablation in liquid ambient, which was developed in our previous works [24–26]. A TiN target was fixed vertically on the wall of a glass vessel filled with 14 mL of analytical grade acetone. A beam (3 mm) from a Yb:KGW laser (1030 nm wavelength, 270 fs pulse duration, 50 μJ pulse energy, 10 kHz repetition rate, TETA 10 model, Avesta, Moscow, Russia) was focused by a 75 mm lens on the surface of the target through a side wall of the vessel. The thickness of the liquid layer from the entrance glass to the target surface was 7 mm.

The ablation duration was 15 min. The ablation vessel was mounted on a platform which performed continuous scanning over a 5 × 5 mm area with the 5 mm s^{-1} speed in order to avoid ablation from the same area. A minor fraction of relatively large (~100 nm) TiN NPs or small amorphous titanium oxide flakes was sedimented by centrifugation (1000 g, 15 min) and removed from solution.

2.3 Coating of Nanoparticles by PEG

The laser-synthesized TiN NPs were functionalized with PEG using modified Stober method. Briefly, 1 mg of TiN NPs was dispersed in 1 mL of 96% ethanol, then 65 mL of distilled water and 20 mL of 30% ammonia hydroxide were added. After thorough ultrasonication, 100 mL of 1 g L^{-1} mPEG-Silane solution in ethanol was quickly dropped to NPs colloid under stirring to start the reaction of silane chains hydrolysis and condensation. Next, NPs were heated to 60 °C for 2 h and further incubated at room temperature (RT) overnight. The obtained TiN-PEG NPs were washed 3 times with ethanol and distilled water via centrifugation at 15000 g for 15 min.

2.4 Characterization of Nanoparticles

Morphology, size and composition of the synthesized TiN NPs were characterized by means of scanning electron microscopy (SEM) system (MAIA 3, Tescan, Czech Republic) coupled with an energy dispersive spectrometry (EDS) detector (X-act, Oxford Instruments, High Wycombe, UK). Electron images were obtained at 30 keV accelerating voltage, while EDS spectra were measured at 15 keV. Hydrodynamic diameter and ζ-potential were measured by dynamic light scattering (DLS) technique using Malvern Zetasizer Nano ZS (Malvern Instruments, UK). Mode values of number-weighted size distributions were used as the hydrodynamic diameter. The evaluation of colloidal stability and ζ-potential in biologically relevant conditions were performed using TiN

NPs preincubated in phosphate buffered saline (PBS) at pH 7.4 for 15 min before the measurement. Smoluchowski approximation was used for ζ-potential calculation. To measure Extinction spectra of TiN NPs colloids were recorded with an Infinite M1000 PRO spectrophotometer (Tecan, Austria).

Protein adsorption on the NPs surface was measured by mixing 100 μg of TiN or TiN-PEG NPs with 1 mg of BSA in PBS and a subsequent incubation at room temperature (RT) overnight. Then, the NPs were washed from unadsorbed proteins 3 times by centrifugation at 10000 g for 15 min. Adsorbed protein quantity was determined using commercial "Total Protein-3-Olvex kit" (#006.003, Olvex diagnosticum, Russia). The kit was calibrated on samples with known quantities of BSA.

Long-term stability of optical properties of nanoparticles was analyzed by measurement of extinction spectra change of NPs in mice serum in a 1 day of incubation. To perform this test, blood was taken from the retroorbital sinus of BALB/c mice, centrifuged at 500 g for 10 min and blood serum was collected. Then, 10 μg of PEG-coated TiN nanoparticles was mixed with 200 μL of serum in plastic tube, ultrasonicated and maintained at room temperature. Extinction spectra of nanoparticle suspension were measured in a 96-well plate with an Tecan Infinite M1000 PRO spectrophotometer.

2.5 Cell Cultures

In vitro tests of TiN and TiN-PEG NPs were performed on comprehensive set of different cell lines, including human HCC1143 (ATCC® CRL-2321), MCF7 (ATCC® HTB-22), SKBR-3 (ATCC® HTB-30), BT474 (ATCC® CRL-3247), A549 (ATCC® CCL-185), HeLa (ATCC® CCL-2), SKOV3-1ip (collection of Laboratory of Molecular Immunology IBCh RAS) and Chinese hamster ovary CHO (collection of Laboratory of Molecular Immunology IBCh RAS). All cell lines were maintained in DMEM medium supplemented with 10% FBS, 2 mM L-glutamine, 50 U mL^{-1} penicillin, and 50 μg mL^{-1}

streptomycin (full culture medium). Cells were incubated under a humidified atmosphere with 5 % CO_2 at 37 °C.

EMT6/P mouse cells were purchased from ECACC (Sigma-Aldrich) and maintained in DMEM medium supplemented with 10 % FBS and 2 mM L-glutamine. Cells were cultured under a humidified atmosphere with 5 % CO_2 at 37 °C, harvested from culture plate with 2 mM EDTA solution, centrifuged at 100 g for 5 min, washed twice with PBS and resuspended in PBS at 10^7 cells mL^{-1} before injection to mice.

2.6 MTT Cytotoxicity Tests

The cytotoxicity of TiN and TiN-PEG NPs was investigated using standard MTT assay. Cells were seeded on a 96-well plate at 10^4 cells per well in 100 μL of DMEM medium supplemented with 10 % FBS and cultured overnight, which corresponds to *ca.* 20% of cell monolayer at the seeding time and *ca.* 30% of monolayer after overnight incubation. Then, NPs dispersed in DMEM at concentrations from 0.03 to 600 μg mL^{-1} were added to the wells to get the final NPs concentration within the 0.015-300 μg mL^{-1} range, which corresponds to ~$3.4 \cdot 10^3$ – $6.8 \cdot 10^7$ TiN NPs per cell or ~ $3 \cdot 10^7$ – $6.1 \cdot 10^{11}$ nm^2 NPs surface area per cell. After that, cells with NPs were incubated for 48 h with a subsequent removal of the medium, followed by the addition of 100 μL MTT solution (0.5 g L^{-1} in DMEM). The prepared samples were incubated at 37 °C for 2 h, then MTT solution was removed, and 100 μL of DMSO was added to the wells. The plate with cells was gently shaken until formazan crystals dissolved completely. Then, optical density at a wavelength of 570 nm was measured for each well using Infinite M1000 PRO microplate reader. Cell viability was presented in percentages normalized to control non-treated cells.

2.7 Flow Cytometry

Flow cytometry was used to analyze potential cell cycle deviations caused by the NPs. To perform the analysis 70-80 % confluent cells were harvested using 2 mM EDTA, re-suspended in a full culture medium, seeded at 12-well flat-bottomed culture plates and incubated overnight under a humidified atmosphere with 5 % CO_2 at 37 °C in DMEM growth medium. Then, TiN or TiN-PEG NPs were added to get final concentration of 30 μg mL^{-1} and the whole mixture was incubated for 48 h. After that, cells were harvested with a 2 mM EDTA solution to 1.5 mL tubes, centrifuged at 100 g for 5 min. Then, 700 μL of ice-cold 70 % ethanol was added to each tube, followed by the incubation for 1 h at +4 °C and the centrifugation at 100 g for 10 min. Next, 200 μL of propidium iodide at 50 μg mL^{-1} and RNAse A at 0.05 g L^{-1} were added. Finally, samples were incubated at RT for 15 min and analyzed with a flow cytometry. DNA content in cell cycle phases was analyzed using a BD Accuri C6 flow cytometer (BD, USA) in FL2 channel (excitation wavelength 488 nm, emission filter 585/40 nm), followed by data analysis in CFlow Plus and FlowJo software.

2.8 Animals

All animal studies were carried out in strict accordance with the provisions of the European Convention for the Protection of Vertebrate Animals Used for Experimental and Other Scientific Purposes and was approved by the Institutional Animal Care and Use Committee of Shemyakin–Ovchinnikov Institute of Bioorganic Chemistry (Moscow, Russia).

Female BALB/c mice with 22-24 g weight were used in the experiments. Animals bearing EMT6/P tumor were used in pharmacokinetic studies. Mice were inoculated into the flank region with 10^6 EMT6/P cells in 100 μL of PBS. Mice with 300 ± 100 mm^3 tumor volume were used in the experiments. Healthy animals without tumor were used for toxicity studies. Mice were anesthetized by an intraperitoneal injection of 40/8 mg/kg

Zoletil/Rometar mixture, followed by NPs injection into the retroorbital sinus. Blood samples for pharmacokinetic and toxicity analysis were taken from the opposite retroorbital sinus.

2.9 Pharmacokinetic and Biodistribution Studies

Pharmacokinetic of TiN and TiN-PEG NPs was studied using inductively coupled plasma mass spectrometry (ICP-MS). A mass-spectrometer (NexION 2000, PerkinElmer, USA) was calibrated before each analysis on samples with known concentrations of NPs (10, 1, 0.1, 0 mg L^{-1}), pre-dissolved in nitric acid. ^{50}Ti peak with calculated lower detection limit 0.015 μg mL^{-1} was used for the analysis.

To study blood circulation of TiN and TiN-PEG NPs we intravenously injected 200 μg of NPs, then 20 μL of blood was taken at 1, 5, 15, 30, 60, 120 and 180 min after the NPs injection. The blood samples were subsequently mixed with 80 μL of concentrated nitric acid and heated to 80 °C for 15 min, followed by 5-fold dilution with water and ICP-MS measurement. TiN quantity was calculated in percentage of the injected dose (% ID) by assuming that weight of the whole mice blood is equal to 7 % of the mice body weight. The area under normalized circulation–time curve (AUC) was calculated during the first 3 h after NPs administration, using a trapezoidal approach.

For biodistribution studies, mice were euthanized by cervical dislocation 3 h after the NPs injection, and liver, spleen, lungs, kidneys, heart, brain, muscle and tumor were extracted and weighted. Then, 100-200 mg of sample tissues were diluted with 3-fold volume of concentrated nitric acid and heated at 80 °C until the solutions became clear. After that, samples were diluted 10-fold with MilliQ water and centrifuged at 1000 g for 5 min before the ICP-MS measurements. Finally, NPs concentrations were normalized to

the total TiN quantity from all measured organs and expressed as percentage of injected dose per gram of tissue (% ID g^{-1}).

2.10 Hemotoxicity

To study hemotoxicity of TiN and TiN-PEG NPs, blood samples were collected with heparin to prevent clotting. For hemolysis assay, red blood cells (RBC) were isolated and washed twice with PBS via centrifugation at 500 g for 3 min. NPs at known concentrations were incubated with RBC diluted to 5 % hematocrit for a 1 h at RT under mild stirring to prevent sedimentation. After the incubation, the supernatant was isolated by centrifugation at 500 g for 5 min to remove RBC, followed by centrifugation at 15000 g for 10 min to remove the NPs. Optical density of the samples at 540 nm was measured using a microplate reader and normalized to a sample incubated in distilled water as a positive control (100 % hemolysis). A control RBC sample, incubated with PBS under similar conditions, was used as a negative control. For agglutination test, RBC were isolated and washed twice with 1 % BSA in PBS via centrifugation at 500 g for 3 min. NPs at known concentrations were incubated with RBC diluted to 1 % hematocrit in 96-well U-shaped plates for 1 h at RT. A sample incubated without NPs was used as a negative control. To make a positive control, RBC were incubated with a rat anti-mouse RBC antibody (TER-119) at final concentration of 25 μg mL^{-1} for 10 min, followed by washing from unbound antibodies and mixing with secondary goat anti-rat antibody at final concentration of 10 μg mL^{-1}. RBC with a sign of agglutination did not form small red dot on the bottom of wells. For hematocrit measurements, TiN and TiN-PEG NPs were intravenously administered in a dose of 6 mg kg^{-1}, followed by the collection of 40 μL of blood into a microhematocrit capillary tube and a subsequent centrifugation in CM-70 hematocrit centrifuge (ELMI, Latvia).

2.11 Toxicity In Vivo

To assess toxicity, TiN and TiN-PEG NPs were intravenously administered at the dose of 6 mg kg^{-1}. Then, mice body weight was recorded every 2 days after the injection for 10 days. During 1^{st} and 7^{th} day after the NPs administration, 200 μL of mice blood was collected without heparin. The following biochemical parameters were determined in mouse serum using microplate reader: aspartate aminotransferase (AST) was determined using a commercial AST-RF-OLVEX kit (#002.001, Olvex Diagnosticum, Russia); alanine aminotransferase (ALT) was determined using a commercial ALT-RF-OLVEX kit (#001.001, Olvex Diagnosticum, Russia); lactate dehydrogenase (LDH) was determined using a commercial LDH-OLVEX kit (#023.001, Olvex Diagnosticum, Russia); UREA was determined using a commercial UREA-2-OLVEX kit (#008.002, Olvex Diagnosticum, Russia); alkaline phosphatase (ALP) was determined using a commercial ALKALINE PHOSPHATASE-2-OLVEX kit (#009.002, Olvex Diagnosticum, Russia).

2.12 Statistical Analysis

At least three independent experiments were conducted for each data point. Results were expressed as mean ± SD. Statistical significance in differences between results was evaluated using a two-tailed Student t-test with unequal variances (Welch's t-test). The differences were considered statistically significant when the p value was less than 0.05 (*), 0.01 (**), 0.001 (***).

3. Results

3.1 Synthesis, Functionalization and Characterization of TiN NPs

To synthesize TiN NPs, we used methods of ultra-short laser ablation and fragmentation in liquid ambient [24,25,27]. Details of experimental procedure are described in the Experimental Section. Laser ablation of the TiN target in acetone resulted in a fast blue coloration of the solution in the ablation chamber (insert in Figure 1a), evidencing the formation of TiN NPs. A typical SEM image of the synthesized NPs along with its size distribution is shown in Figure 1a (more SEM images are shown in Figure S1 in Supplementary data). One can see that the NPs had spherical shape, while the size distribution was lognormal with 25 nm mode size in accordance with our previous studies [24]. EDS analysis (Figure 1b) qualitatively confirmed chemical composition of the synthesized TiN NPs. Here, main signals presented in the spectrum corresponded to nitrogen (N) and titanium (Ti), while small oxygen (O) signal could be explained by surface oxidation of the NPs. Large silicon (Si) peak in the spectrum originated from the Si substrate, while carbon (C) signal was related to organic contamination of microscope vacuum chamber or the sample itself due to the presence of traces of acetone after its evaporation.

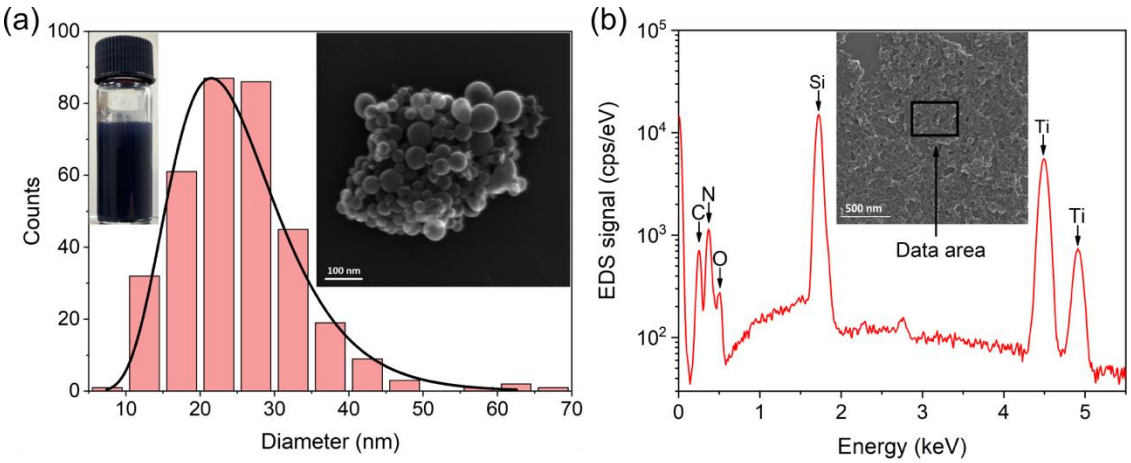

Figure 1. Physicochemical characterization of bare TiN NPs. (a) A typical SEM image and corresponding size distribution of TiN NPs (350 individual NPs were measured) synthesized by fs laser ablation. The insert on the left side demonstrates a photo of TiN NPs colloidal solution. (b) EDS spectrum of the synthesized NPs illustrating strong titanium and nitrogen signals from NPs. A small oxygen peak can be related to a minor

oxidation of the NPs surface. A silicon peak originates from a Si substrate, while the carbon signal is related to organic contamination of the vacuum chamber or solvent residue.

Colloidal stability of TiN NPs solutions was high both in acetone and after transfer to deionized water without addition of any stabilizing agents, which is related to a strong negative charge of TiN NPs. Since projected biomedical applications require colloidal stability of NPs under physiological conditions, we dispersed TiN NPs in PBS, which has similar conductivity and ion composition of blood serum and thus can be considered as a good model to simulate physiological ambience for colloidal stability tests. Our results showed that after dispersion in PBS, bare TiN NPs aggregated and precipitated within tens of minutes. To improve colloidal stability of TiN NPs and make them less visible for the immune systems, we covered them by a hydrophilic PEG, which is frequently used for these purposes [28,29]. It is known that dense conformations of PEG chains on NPs surface can lead to prolongation of NPs circulation in the bloodstream and their enhanced delivery to a therapeutic target [28].

The coverage of TiN NPs by PEG (PEGylation) was done using Stober process as described in Experimental Section and schematically shown in Figure 2a. We used a high molar excess of 2 kDa mPEG-Silane molecules to obtain a dense coating of PEG on the NPs surface. The efficiency of the PEGylation was assessed by a series of tests. First, we measured hydrodynamic sizes of bare TiN NPs and NPs covered by PEG (TiN-PEG NPs) in water and PBS. Before the modification TiN NPs had the hydrodynamic diameter of 79 nm (mode value), while the PEGylation led to its increase up to 91 nm (Figure 2b), which confirmed a successful coupling of PEG chains to the TiN surface. It is important that TiN-PEG NPs had better colloidal stability in physiologically relevant conditions as they did not change their hydrodynamic size after dispersion in PBS. For comparison, the

size of uncoated TiN NPs gradually increased and reach 750 nm under their aging in PBS for ten minutes. It was also found that the PEGylation changed ζ-potential of TiN NPs (Figure 2c). Originally having a negative ζ-potential (-29.3 ± 10 mV), the NPs changed it to almost neutral values (-4.9 ± 7.2 mV), which was consistent with surface coating by neutral PEG molecules [30].

We additionally found that the PEGylation can decrease adsorption of nonspecific proteins on the TiN NPs surface. TiN and TiN-PEG NPs were incubated in BSA solution for 12 h and then washed from unbound proteins. A Pyrogallic Red technique was then used to measure the quantity of adsorbed albumin. The amount of BSA adsorbed to the bare TiN NPs surface was approximately 6 mg per gram of NPs, as shown in Figure 2d. At the same time, no adsorbed BSA was detected in the sample with TiN-PEG NPs. This drastic difference confirmed that PEGylation reduces absorption of proteins on NPs surface.

Finally, the examination of optical properties revealed broad plasmonic peak centered at 700 nm for both TiN and TiN-PEG NPs (Figure 2e). The PEGylation of TiN NPs changed the optical properties insignificantly: it led only to a slight (5 %) decrease of the extinction peak and a 20 nm shift of its profile toward longer wavelengths. Moreover, TiN-PEG NPs preserved their optical properties in blood serum for at least one day (Figure S2).

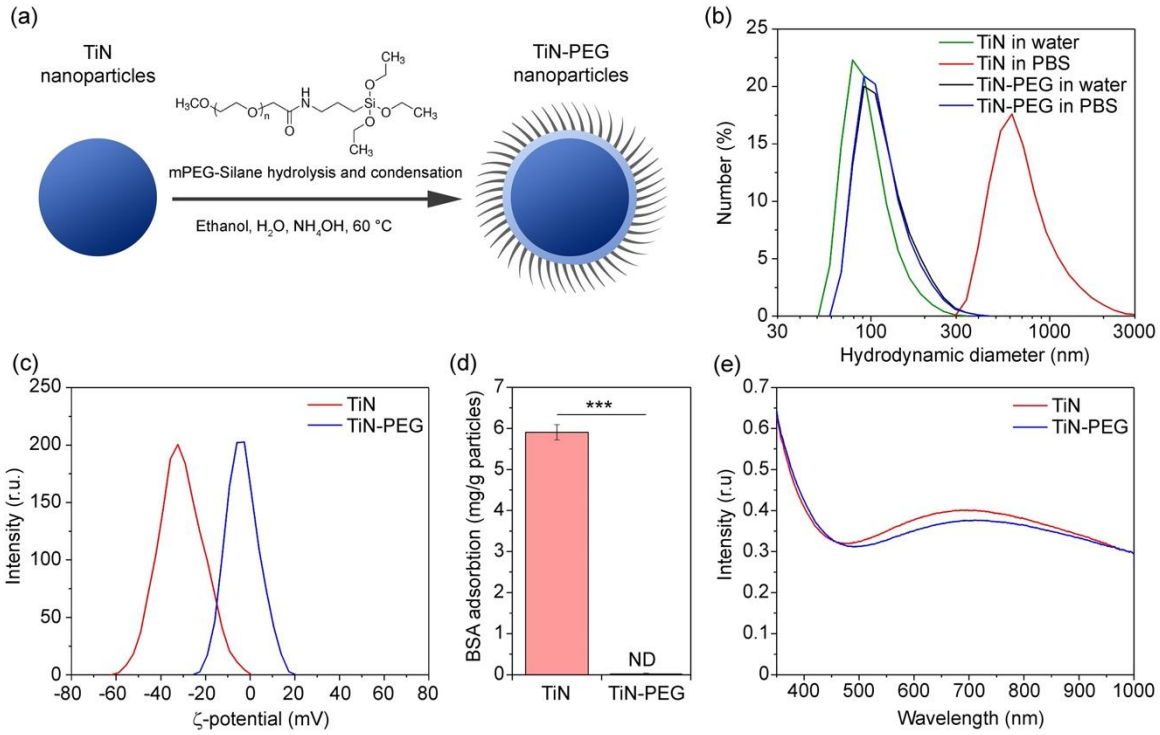

Figure 2. Fabrication of TiN-PEG NPs and their physicochemical properties. (a) Scheme of modification of TiN NPs surface with PEG. (b) Number-weighted hydrodynamic size distributions of TiN and TiN-PEG NPs in water and PBS. (c) ζ-potential distributions of bare TiN and TiN-PEG NPs in PBS. (d) Amount of BSA adsorbed per gram of TiN and TiN-PEG NPs. ND – not detected (n=3). (e) Optical extinction spectra of TiN and TiN-PEG NPs. The statistical significance was evaluated using Welch's t-test (*** $P < 0.001$).

3.2 Evaluation of Nanoparticles Toxicity In Vitro

To evaluate cytotoxicity of NPs *in vitro*, we performed a comprehensive study including MTT analysis of 8 cell lines of different tissue (breast, cervix, ovary) and organism (human, hamster) origin, namely, HCC1143 – mammary breast carcinoma, MCF7 – mammary breast adenocarcinoma, SKBR-3 – mammary breast adenocarcinoma, BT474 – mammary ductal adenocarcinoma, A549 – lung carcinoma, HeLa – cervical adenocarcinoma, SKOV3-1ip – ovarian adenocarcinoma and CHO – Chinese hamster ovarian cells. MTT test is a colorimetric assay used for the estimation of cell metabolic activity profiting from the ability of NAD(P)H-dependent cellular oxidoreductases to

reduce the tetrazolium dye MTT to its insoluble analogue formazan which has characteristic optical absorption at 570 nm. Cells were incubated with 0.015-300 μg mL^{-1} solutions of TiN and TiN-PEG NPs for 48 h and subsequently evaluated with MTT. As shown in Figure 3a, all cell lines demonstrated more than 65 % viability after the treatment with both types of NPs up to 30 μg mL^{-1} concentration, more than 70 % viability up to 3 μg mL^{-1}, and more than 73 % viability up to 0.4 μg mL^{-1}. There was no significant difference in cell viability after treatment with either bare TiN or TiN-PEG NPs for all cell lines. However, a slight decrease of cytotoxicity of TiN-PEG NPs as compared to bare TiN NPs was observed for 3 cell lines of different origin: HCC1143, A549, CHO.

Note that in some cases results of MTT assay can underestimate cytotoxic effect of examined nano agents due to the fact that cell metabolism, which is tested by the MTT reduction, can continue to operate for a certain time period even after the cell death. Moreover, formazan, which is the substance that is spectroscopically probed in the MTT test, can also be produced by compounds that cause perturbations in phase distribution of cell cycles [31]. To exclude possible unambiguity of MTT test results, flow cytometric analysis using propidium iodide DNA staining was applied to evaluate possible alterations of cell cycle after treatment with both types of NPs. Results of flow cytometry analysis are presented in Figure 3b,c. One can see that there was almost complete absence of changes in the G1/G0, S and G2/M phases of the cell cycle, and no cell cycle arrest was observed upon exposure to either TiN or TiN-PEG NPs for all tested cell lines. However, the PEGylation of TiN NPs significantly reduced the percentage of cells in sub-G1 peak (containing cells with fragmented DNA, e.g. apoptotic cells). Namely, the sub-G1 percentage of cells treated with TiN-PEG NPs in comparison with TiN NPs decreased from 6.1 ± 0.6 to 3.3 ± 0.3 % for HCC1134 cells, from 8.1 ± 0.1 to 6.8 ± 0.3 % for MCF7

cells, from 6.9 ± 0.6 to 4.3 ± 0.2 % for SKBR-3 cells, from 8.3 ± 0.7 to 3.3 ± 0.1 % for BT474 cells, from 3.5 ± 0.2 to 1.9 ± 0.1 % for A549 cells, from 3.1 ± 0.1 to 1.9 ± 0.1 % for SKOV3-1ip cells, and from 4.2 ± 0.3 to 1.5 ± 0.1 % for CHO cell line. Therefore, for all cell lines treated with TiN-PEG NPs percentage of cells in sub-G1 peaks was comparable with that for non-treated cells, thus indicating the efficiency of NPs PEGylation for cytotoxicity reduction.

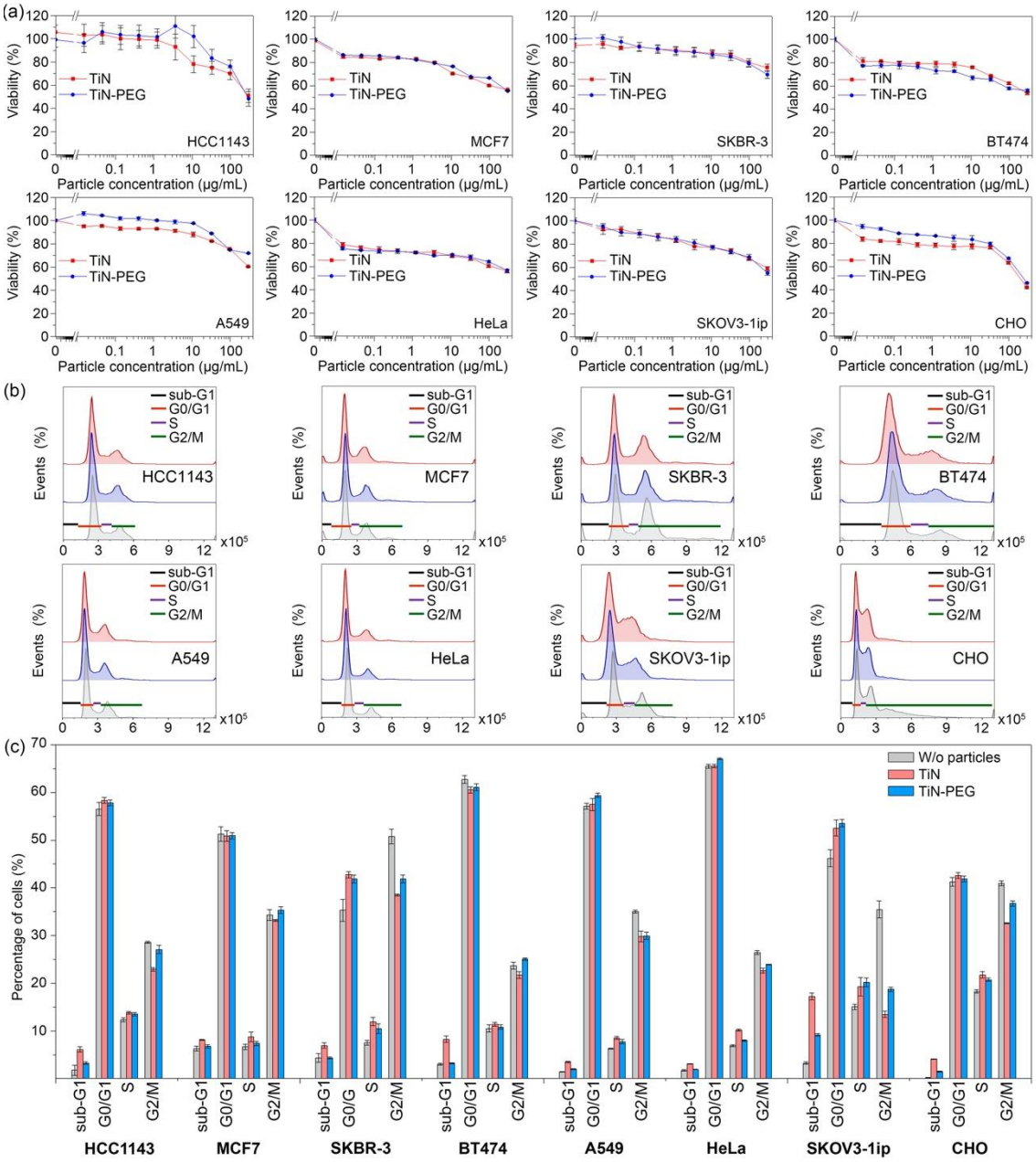

Figure 3. *In vitro* cytotoxicity study of TiN and TiN-PEG NPs using MTT and flow cytometry assays on 8 cell lines including HCC1143, MCF7, SKBR-3, BT474, A549,

HeLa, SKOV3-1ip and CHO cells. (a) MTT test results for each cell line after 48 h of NPs treatment. (n=3). (b) Cell cycle analysis by flow cytometry. Histograms demonstrate the analysis of non-treated cells (gray filled histograms), cells treated with TiN NPs (red open histograms) and cells treated with TiN-PEG NPs (blue open histograms). (c) Quantification of cell cycle analysis for non-treated cells (grey) and cells after their treatment with TiN (red) or TiN-PEG (blue) NPs indicating percentage of cells in sub-G1, G1/G0, S, G2/M phases of cell cycle. (n=3).

3.3 Blood Circulation and Biodistribution of TiN Nanoparticles

Passive tumor targeting ability of both bare TiN and TiN-PEG NPs was assessed *in vivo* using a murine model. Mice were inoculated subcutaneously with EMT6/P mammary carcinoma cells. When the tumor size was 300 ± 100 mm^3 we injected NPs and studied their pharmacokinetic and biodistribution using ICP-MS. NPs concentrations in the bloodstream were determined between 1 min and 3 h after the administration using a blood-sampling technique. As shown in Figure 4a, bare TiN NPs had a short half-life in the bloodstream and were rapidly cleared, which was probably due to their low colloidal stability under physiological conditions. In particular, we observed only 16 % ID of NPs in the bloodstream 1 min after the injection, while within the first 30 minutes the NPs were fully eliminated. However, the PEGylation of TiN NPs allowed us to drastically improve their circulation time as we were able to detect the presence of TiN-PEG NPs in the bloodstream 1 h after the administration.

To quantitatively compare the circulation kinetics of both NPs types, we calculated their area under the curve (AUC) during the first 3 h following the administration (Figure 4b). AUC is commonly used for kinetics analysis, when the curve cannot be fitted by an exponential function due a low number of data points or complex pharmacokinetic behavior. PEGylation of TiN NPs resulted in more than 7-fold increase

of AUC for TiN-PEG NPs as compared to bare TiN NPs. Such a significant prolongation of NPs circulation can be explained by “stealth” properties of PEG polymer.

To study the biodistribution of NPs we sacrificed mice and collected all major organs as well as tumor 3 h after the administration when all NPs were removed from the bloodstream. The results of the biodistribution analysis are shown in Figure 4c. It is visible that laser-synthesized NPs were mainly accumulated in liver and spleen: 92.4 ± 1.1 and 50.5 ± 8.3 ID g^{-1} for bare TiN NPs, and 91.8 ± 0.4 and 46.2 ± 6 ID g^{-1} for TiN-PEG NPs, respectively. At the same time, we observed a significant 2.2-fold increased amount of TiN-PEG NPs in the tumor as compared to bare TiN NPs (2.4 ± 0.4 vs. 1.1 ± 0.2 % ID g^{-1}). This result can be explained by increased blood circulation time of TiN-PEG NPs, which made possible their efficient delivery to tumor and accumulation via enhanced permeability and retention (EPR) effect [32]. Moreover, we observed an extremely low (comparable to the noise level) concentrations of NPs in brain, muscles and kidney. This fact additionally suggests that the NPs were indeed cleared from the bloodstream within 3 hours, but not renally excreted due to their relatively large size

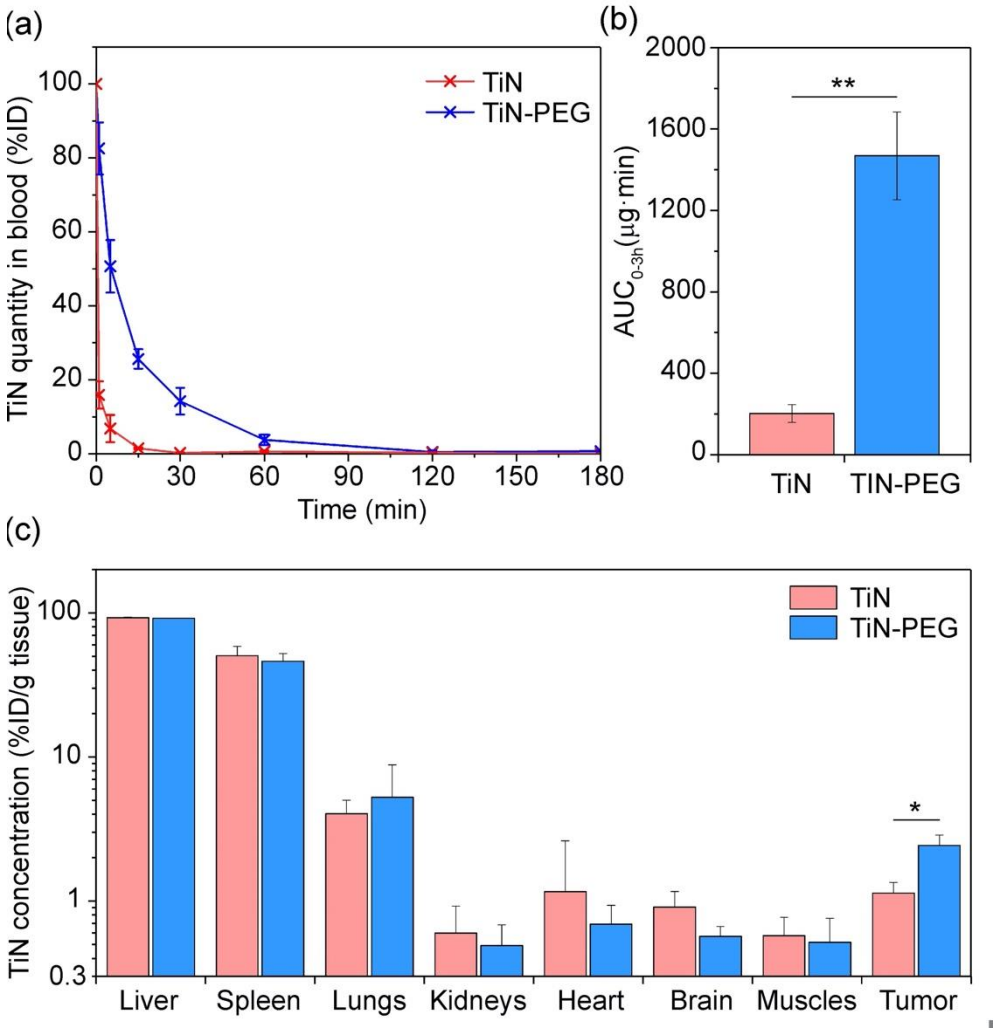

Figure 4. Pharmacokinetic and biodistribution of TiN (red) and TiN-PEG (blue) NPs. (a) Blood circulation kinetics determined by ICP-MS. (n=3). (b) Area under the curve (AUC) of circulation kinetics during the first 3 h after the NPs administration. (n=3). (c) Biodistribution of NPs in organs of BALB/c mice. (n=3). The statistical significance was evaluated using Welch's -test (* $P < 0.05$; ** $P < 0.01$).

3.4 Blood Tests and Nanoparticles Toxicity In Vivo

In the bloodstream NPs can interact with various blood cells, including erythrocytes, and damage them. To test possible toxicity of NPs with respect to red blood cells (RBC), we carried out several blood assays, including hemolysis analysis, agglutination tests and hematocrit variation.

RBC hemolysis detection is based on a spectrophotometric measurement of hemoglobin released from erythrocytes after NPs stress-induced membrane disruption. We found that the PEGylation of TiN NPs significantly reduced RBC hemolysis at NPs concentrations above 1 mg mL^{-1} (Figure 5a). In particular, at a NPs/RBC ratio of 1 mg mL^{-1}, TiN-PEG NPs caused more than 2-fold reduced hemoglobin release as compared to bare TiN NPs, while at low NPs/RBC ratio (0.1 mg mL^{-1}) the hemolytic activity of both types of NPs was negligible. A standard RBC agglutination assay was performed in a round-bottom 96-well plate. In the absence of agglutination erythrocytes sediment and forms a red dot in the center of the well (Figure 5b, negative control), while in the case of agglutination RBC are distributed over the whole surface of the well (Figure 5b, positive control). The agglutination test demonstrated that at low NPs concentrations (up to 1 mg mL^{-1}), both bare TiN and TiN-PEG NPs did not cause agglutination, while at large 10 mg mL^{-1} dose TiN NPs had higher erythrocyte aggregation potential, confirming that the PEGylation can substantially reduce the possibility of RBC agglutination. It should be noted that results of *in vitro* tests (hemolysis and agglutination) can demonstrate slightly different toxicity levels compared with *in vivo* studies [33]. One of the reasons of such a difference is related to the presence of plasma proteins in the bloodstream, which can coat the NPs and thus alter their interaction with RBC.

To avoid misinterpretations, we additionally monitored variations of hematocrit after NPs administration *in vivo*, which typically evidence erythrocyte damage, caused by hemolysis, agglutination and other reasons. We found that TiN NPs caused a statistically significant decrease in hematocrit level from 50.8 to 48.4 % 3 h after the NPs injection, but this level returned to normal values 3 days after the NPs injection (Figure 5c). At the same time, the administration of TiN-PEG NPs did not cause any statistically significant

hematocrit variation, which confirmed a significant reduction of hemotoxicity due to the PEGylation process.

Finally, we assessed possible long-term toxicity due to the administration of TiN and TiN-PEG NPs. Here, mice weight and blood biochemical parameters were monitored. As shown in Figure 5d, we did not observe any statistically significant variations in weight of mice from control and treated groups during the whole duration of the experiment (10 days). We also did not observe any signs of abnormal behavior in all groups. Blood biochemical analysis was performed during the first and seventh day after the intravenous administration of NPs. Tests included measurements of several parameters: aspartate aminotransferase (AST); alanine aminotransferase (ALT); alkaline phosphatase (ALP); lactate dehydrogenase (LDH); creatinine (CREA) and blood urea (UREA), which are standard stress-markers for the diagnosis of liver, heart and kidney injury. As shown in Figure 5e, no statistically significant difference in any of these parameters for mice from the control group and group treated by TiN and TiN-PEG NPs was observed.

In general, results of our study indicate a low toxicity of laser-synthesized TiN NPs *in vivo*. Mild hemotoxicity of bare TiN NPs could be due to NPs aggregation in blood, but the coating of NPs with PEG polymer significantly reduced such drawbacks and made NPs safe for use in biomedical applications.

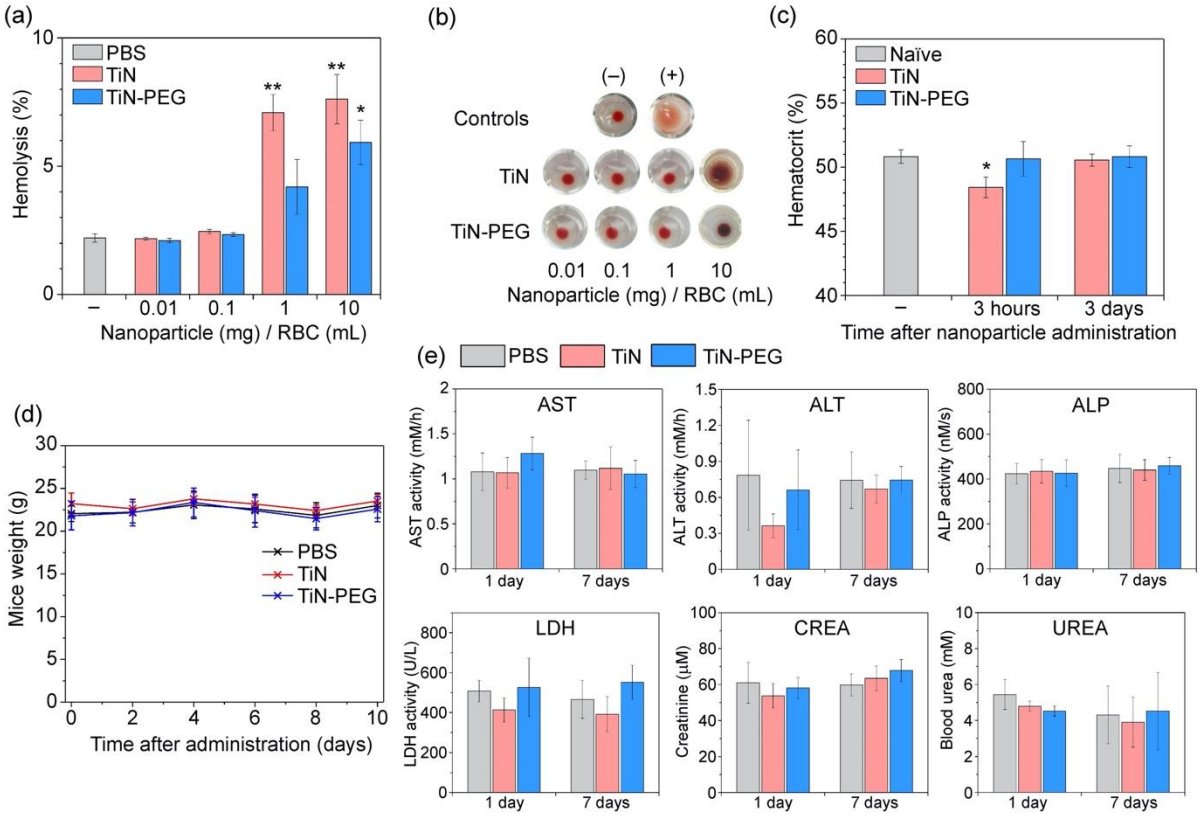

Figure 5. Blood tests and long-term toxicity of bare TiN (red) and TiN-PEG (blue) NPs. (a) Percentage of *in vitro* erythrocytes lysis after the incubation with NPs. (n=3). (b) Round-bottom well assay of RBC agglutination caused by various concentrations of TiN and TiN-PEG NPs; (-) control corresponds to RBC incubated in PBS buffer only, (+) control corresponds to RBC incubated in rat anti-mouse RBC TER-119 antibody mixed with goat anti-rat secondary antibody. Precipitation of erythrocytes into the red dot means no agglutination, while aggregated cells form diffuse disk over the well surface. (c) Hematocrit evolution in mice administered with the NPs. (n=6). (d) Kinetics of mice weight after administration of NPs solution or equal amount of PBS. (n=4). (e) Biochemical blood enzymes tests during the 1st and 7th day after the administration of PBS (grey), TiN (red) or TiN-PEG (blue) NPs: activity of aspartate transaminase (AST), alanine transaminase (ALT), alkaline phosphatase (ALP), lactate dehydrogenase (LDH); creatinine level (CREA), urea in blood (UREA). (n=4). Asterisks indicate significant difference from the control (grey bar in each graph): Welch's t-test (* $P < 0.05$; ** $P < 0.01$).

4. Discussion

Laser ablation in liquids provides a fast, simple and scalable way for synthesis of various NPs types (for review, see, e.g. [34,35]). This method was earlier applied for the synthesis of a plethora of nanomaterials, including gold [36], silicon [37], carbon [38], ZnO-based [39] NPs and carbon nanotubes [40]. In this study, we applied methods of fs laser ablation for the fabrication of TiN NPs according to a procedure developed in our earlier study [23]. Since the proposed research is material-oriented, we used a relatively simple experimental arrangement, which does not make possible a high production rate, but this rate can be easily improved up to 4 g h^{-1} of NPs by the employment of advanced laser ablation setups [41]. Note that clinical trials of cancer PTT treatment with chemically-synthesized gold-based nano shells required administration of approximately 3 g of NPs per patient [42]. Taking into account that photothermal conversion efficacy of TiN NPs is even higher than that of gold nano shells [43], we can conclude that existing laboratory laser ablation setups can produce enough NPs for the treatment of several humans per just one hour. As another important advantage, laser ablative synthesis can become cheaper than chemical synthesis pathways under large production scale when the productivity values are higher 0.55 g h^{-1} [44]. Based on characteristics of nanomaterials and economic analysis, laser-synthesized TiN NPs present a new promising candidate for biomedical applications. However, evaluation of *in vivo* cytotoxicity of laser synthesized TiN NPs has not yet been done and this study was conceived as the first attempt to fill this gap.

The mean size of TiN NPs used in this study was about 25 nm with 20 nm full width at half maximum (FWHM) as shown in Figure 1a. Spectral position of plasmonic feature of TiN NPs in this size range almost does not depend on NPs size [17], therefore we considered our size distribution as narrow enough. However, it is possible to selectively sort laser-synthesized NPs in this size range (with FWHM 10 nm or lower) by

sedimentation-based centrifugation [45]. Moreover, this NPs size looks favorable for biomedical applications as it is small enough to efficiently accumulate in tumor via passive mechanism based on EPR effect [32], but not too small to be rapidly cleared from the blood circulation via renal filtration [46]. A successful delivery of NPs to the tumor depends on several factors including, NPs colloidal stability in the bloodstream and the rate of NPs sequestering by cells of the immune system [28]. Both parameters can be much improved by NPs surface modification with certain biopolymers. Since PEG is one of most efficient polymers for this task, it was selected for surface modification of laser-synthesized TiN NPs in our study. As follows from our tests, the coating of NPs by PEG lead to a significant improvement of colloidal stability due to the change of stabilization mechanism from electrostatic, which becomes inefficient in the case of highly conductive fluids, to a steric one.

A successful grafting of PEG on TiN NPs surface was verified by several observations: an improved colloidal stability of TiN-PEG NPs in PBS (Figure 2b); a slight increase of NPs hydrodynamic size (Figure 2b); and a change of surface potential toward neutral values (Figure 2c). The decrease of the absolute value of NPs ζ-potential is an important factor, which reduces adsorption of serum proteins [47] and thus increases circulation time of NPs in the bloodstream. We assessed the influence of PEGylation on nonspecific adsorption of proteins using BSA and found that bare TiN NPs adsorbed up to 6 mg of proteins per g of NPs, while the amount of proteins adsorbed on TiN-PEG NPs was undetectable (Figure 2d), which additionally confirmed good protective properties of PEG coating. As another important result, the PEGylation almost did not affect optical properties of laser-synthesized NPs (Figure 2e). This fact additionally confirms that strong extinction of TiN NPs in the IR region should be attributed to individual properties

of TiN NPs and not to their collective excitation, which can cause a similar effect for other plasmonic NPs such as gold [48].

Pharmacokinetic studies confirmed that the PEGylation of TiN NPs is indeed beneficial for the prolongation of their circulation time in blood. Current explanation of "stealth" properties of such modified NPs is based on a reduced interaction of PEG with opsonins and an increased adsorption from serum of certain dysopsonins such as clusterin and apolipoproteins [49]. TiN-PEG NPs circulated in the bloodstream 7 times longer than the bare ones. After elimination from the bloodstream both TiN and TiN-PEG NPs accumulated preferentially in liver and spleen, major organs of mononuclear phagocyte system, due to the presence of Kupffer cells in liver and macrophages in spleen. These organs usually eliminate of up to 98 % NPs [50]. At the same time, we found 2.2-times better delivery of PEGylated TiN NPs to tumor as compared to uncoated ones. We believe that preferential accumulation of NPs in tumor is due to the EPR effect [32], which generally becomes more efficient for sufficiently small (<100 nm) NPs [51]. In general, a successful delivery of TiN-PEG NPs to tumor confirmed that laser-synthesized NPs are small enough to reach the tumor through vascular pores even after their coating with PEG.

The passive delivery of plasma-synthesized TiN NPs to tumor at concentrations, sufficient for photo acoustic imaging (PAI) and PTT applications, was recently demonstrated [15,19]. However, a mass-spectrometric investigation of NPs delivery in these studies revealed nearly the same level of signal from tumor, kidney and other healthy tissues. In our work, even uncoated TiN NPs showed almost 2-times higher accumulation in tumor node than in muscles and kidneys, while the PEGylation further enhanced the difference as the NPs circulated in bloodstream for a longer time and had more chances to reach their target in the organism. We believe that the recorded substantial increase in efficiency of NPs delivery to the tumor in the case of laser-

synthesized TiN NPs can be explained by a much narrower size dispersion in the absence of any aggregations (in the case of plasma synthesis, the NPs are typically size-dispersed and partially aggregated [19,23]). We suppose that a further prolongation of the blood circulation time can be achieved via the modification of density and length of the PEG coating [28,49] or the combination of PEGylation with another "stealth" strategies [52,53].

TiN NPs for cancer therapy and imaging applications are supposed to have a low impact on healthy tissues and cells in the organism. Here, we performed a comprehensive study of toxicity of TiN NPs, which involved eight cell lines from different tissues and organisms. It was shown that cells metabolic activity, estimated by the ability of NAD(P)H-dependent cellular oxidoreductases to reduce the tetrazolium dye MTT, did not change significantly under the incubation of both TiN and TiN-PEG NPs, while TiN-PEG NPs demonstrated a slight decrease of cytotoxicity in comparison with the unmodified counterparts. Moreover, we showed that the PEGylation of TiN NPs significantly reduced the percentage of cells in sub-G1 region, which contains cells with fragmented DNA, e.g. apoptotic ones. Apoptosis, induced by nanoparticles is thought to be occurred by 3 distinct pathways, involving activation of death transmembrane receptor, inducing of mitochondrial damage or the endoplasmic reticulum injury [54]. Usually nanoparticle cause apoptosis by reactive oxygen species generation and mitochondrial damage [55] and sometimes by endoplasmic reticulum stress [56]. However, the mechanism of DNA damage of cells in sub-G1 region, most probably apoptotic ones, should be further thoroughly investigated.

The interaction of intravenously administered drugs with blood cells presents one of key data to evaluate their acute toxicity. To assess prospects of laser-synthesized TiN NPs, we carried out *in vitro* tests on the hemolysis and agglutination of red blood cells,

as well as measured hematocrit level *in vivo*. Our results demonstrated that at high doses of TiN NPs their PEGylation significantly reduced the hemolysis of RBC and prevented their agglutination *in vitro*. Such a result can be explained by PEG-related inhibition of NPs binding and uptake by macrophages and other cells [57]. A high efficiency of PEGylation was demonstrated *in vivo*, where TiN-PEG NPs did not cause a drop in the number of circulating red blood cells, which contrasted to results of similar tests using uncoated TiN NPs.

Although TiN NPs were mostly captured in liver and spleen, while products of their degradation were supposed to be eliminated via kidneys, we did not find signs of damage of these organs. Indeed, blood biochemical parameters associated with the injury of liver, heart and kidneys (AST, ALT, ALP, LDH, CREA, and UREA) were invariable within acceptable limits, while weight and behavior of animals remained unchanged and comparable with relevant parameters of mice from the control group. Taken together, our results showed that *in vivo* administration of TiN-PEG NPs at concentrations up to 6 mg kg^{-1} did not cause acute toxicity to mice. Note that the last point of *in vivo* toxicity analysis was measured during the 7^{th} day after the NPs administration. To decisively conclude on long-term toxicity of laser-synthesized TiN NPs, an additional comprehensive study is required. It should be also noted that TiN NPs are supposed to degrade into titanium dioxide (TiO_2), which also does not exhibit toxic properties at used concentrations [58].The degradation occur at time scale that exceeds at least one day (Figure S2), therefore TiN NPs can preserve their useful optical properties *in vivo* long enough for therapeutic applications. Moreover, most of other known compositions of titanium are very stable against corrosion and, therefore are low toxic materials, while some of them are even authorized for use with humans for medical applications [59].

Thus, based on results on *in vitro* and *in vivo* tests, we can conclude that laser-synthesized titanium nitride-based NPs present a safe nanoformulation for future biomedical applications.

It is worth noting that the presented research continues a cycle of studies devoted to the assessment of novel nanomaterials prepared by "green" laser-ablative synthesis in biological systems. In earlier studies [36,60], we already evaluated laser-synthesized Au NPs presenting another promising object for a variety of biomedical applications, including the treatment of neurodegenerative diseases [61], energy converters for pacemakers [62], probes in SERS-based identification of target biomolecules [63,64]. As follows from our analysis, Au NPs also present a safe object, which does not cause any damage of organs or tissues despite their residual accumulation in organs of mononuclear phagocyte system [36]. In another series of studies [29,37,65], we assessed laser-synthesized silicon (Si) NPs, whose intrinsic semiconductor properties make possible a series of unique imaging [66] and therapy [67] functionalities. Our evaluation showed that Si NPs are not only safe, but also biodegradable as they can rapidly decay into orthosilicic acid and excrete from the organism with the urine [65]. In contrast to Au- and Si-based NPs, which have already been widely studied and explored in biomedical applications [1,2], TiN NPs present a new material, which however has superior photothermal and photoacoustic characteristics compared to other plasmonic counterparts and thus can radically advance cancer phototheranostic modalities.

5. Conclusion

This study presents the first assessment of safety, biodistribution and pharmacokinetics of laser-synthesized TiN NPs. It is shown that bare TiN NPs have low toxicity both *in vitro* and *in vivo*, while their coating with PEG can additionally improve the toxicity profile by minimizing the fraction of apoptotic cells *in vitro* and hemotoxicity *in vivo*,

enhancing colloidal stability in biologically relevant environment to increase circulation time of NPs in bloodstream and enhance efficiency of their passive delivery to tumor target. After *in vivo* administration in small animal model, the NPs were mainly accumulated in liver and spleen, but did not cause any acute toxicity at high concentrations up to 6 mg kg^{-1}, which was confirmed by the invariability of blood biochemical parameters related to liver, heart and kidneys functions (AST, ALT, ALP, LDH, CREA, and UREA), stability of weight and behavior of animals compared to the control mice group. The presented results evidence a high safety of laser-synthesized TiN NPs for biological systems in vitro and in vivo, which gives a promise for the development of novel phototherapy and imaging modalities profiting from superior properties of TiN NPs compared to other plasmonic counterparts.

Acknowledgements

The authors acknowledge contribution of the Russian Science Foundation (Project 19-72-30012) for fabrication of nanomaterial, support from the Russian Foundation for Basic Research (Project No. 20-34-70136) for cell culture and toxicity studies and a support from MEPhI Academic Excellence Project (Agreement with the Ministry of Education and Science of the Russian Federation of 27.08.2013, project #02.a03.21.0005) for providing the research equipment and the related scientific infrastructure.

Disclosure statement

No potential conflict of interest was reported by the authors.

References

[1] P.N. Prasad, Introduction to Nanomedicine and Nanobioengineering: Transforming Healthcare with Nanotechnology, Wiley, New York, 2012.

[2] L. Dykman, N. Khlebtsov, Gold nanoparticles in biomedical applications: recent advances and perspectives, Chemical Society reviews 41 (2012) 2256–2282. https://doi.org/10.1039/c1cs15166e.

[3] P.K. Jain, K.S. Lee, I.H. El-Sayed, M.A. El-Sayed, Calculated absorption and scattering properties of gold nanoparticles of different size, shape, and composition: applications in biological imaging and biomedicine, The journal of physical chemistry. B 110 (2006) 7238–7248. https://doi.org/10.1021/jp057170o.

[4] V. Myroshnychenko, J. Rodríguez-Fernández, I. Pastoriza-Santos, A.M. Funston, C. Novo, P. Mulvaney, L.M. Liz-Marzán, F.J. García de Abajo, Modelling the optical response of gold nanoparticles, Chemical Society reviews 37 (2008) 1792–1805. https://doi.org/10.1039/b711486a.

[5] L.R. Hirsch, R.J. Stafford, J.A. Bankson, S.R. Sershen, B. Rivera, R.E. Price, J.D. Hazle, N.J. Halas, J.L. West, Nanoshell-mediated near-infrared thermal therapy of tumors under magnetic resonance guidance, Proceedings of the National Academy of Sciences of the United States of America 100 (2003) 13549–13554. https://doi.org/10.1073/pnas.2232479100.

[6] P.K. Jain, X. Huang, I.H. El-Sayed, M.A. El-Sayed, Noble metals on the nanoscale: optical and photothermal properties and some applications in imaging, sensing, biology, and medicine, Accounts of chemical research 41 (2008) 1578–1586. https://doi.org/10.1021/ar7002804.

[7] M.S. Jabir, U.M. Nayef, W.K. Abdulkadhim, G.M. Sulaiman, Supermagnetic Fe 3 O 4 -PEG nanoparticles combined with NIR laser and alternating magnetic field as potent anti-cancer agent against human ovarian cancer cells, Mater. Res. Express 6 (2019) 115412. https://doi.org/10.1088/2053-1591/ab50a0.

[8] S. Toraya-Brown, S. Fiering, Local tumour hyperthermia as immunotherapy for metastatic cancer, International journal of hyperthermia the official journal of European Society for Hyperthermic Oncology, North American Hyperthermia Group 30 (2014) 531–539. https://doi.org/10.3109/02656736.2014.968640.

[9] A.M. Gobin, M.H. Lee, N.J. Halas, W.D. James, R.A. Drezek, J.L. West, Near-infrared resonant nanoshells for combined optical imaging and photothermal cancer therapy, Nano letters 7 (2007) 1929–1934. https://doi.org/10.1021/nl070610y.

[10] S. Gargiulo, S. Albanese, M. Mancini, State-of-the-Art Preclinical Photoacoustic Imaging in Oncology: Recent Advances in Cancer Theranostics, Contrast media & molecular imaging 2019 (2019) 5080267. https://doi.org/10.1155/2019/5080267.

[11] G.M. Sulaiman, H.M. Waheeb, M.S. Jabir, S.H. Khazaal, Y.H. Dewir, Y. Naidoo, Hesperidin Loaded on Gold Nanoparticles as a Drug Delivery System for a Successful Biocompatible, Anti-Cancer, Anti-Inflammatory and Phagocytosis Inducer Model, Scientific reports 10 (2020) 9362. https://doi.org/10.1038/s41598-020-66419-6.

[12] W.D. James, L.R. Hirsch, J.L. West, P.D. O'Neal, J.D. Payne, Application of INAA to the build-up and clearance of gold nanoshells in clinical studies in mice, J Radioanal Nucl Chem 271 (2007) 455–459. https://doi.org/10.1007/s10967-007-0230-1.

[13] S. Link, C. Burda, M.B. Mohamed, B. Nikoobakht, M.A. El-Sayed, Laser Photothermal Melting and Fragmentation of Gold Nanorods: Energy and Laser Pulse-Width Dependence, J. Phys. Chem. A 103 (1999) 1165–1170. https://doi.org/10.1021/jp983141k.

[14] H. Petrova, J. Perez Juste, I. Pastoriza-Santos, G.V. Hartland, L.M. Liz-Marzán, P. Mulvaney, On the temperature stability of gold nanorods: comparison between thermal and ultrafast laser-induced heating, Physical chemistry chemical physics PCCP 8 (2006) 814–821. https://doi.org/10.1039/b514644e.

[15] C. Wang, C. Dai, Z. Hu, H. Li, L. Yu, H. Lin, J. Bai, Y. Chen, Photonic cancer nanomedicine using the near infrared-II biowindow enabled by biocompatible titanium nitride nanoplatforms, Nanoscale horizons 4 (2019) 415–425. https://doi.org/10.1039/c8nh00299a.

[16] A. Boltasseva, V.M. Shalaev, Materials science. All that glitters need not be gold, Science 347 (2015) 1308–1310. https://doi.org/10.1126/science.aaa8282.

[17] U. Guler, V.M. Shalaev, A. Boltasseva, Nanoparticle plasmonics: going practical with transition metal nitrides, Materials Today 18 (2015) 227–237. https://doi.org/10.1016/j.mattod.2014.10.039.

[18] A. Lalisse, G. Tessier, J. Plain, G. Baffou, Plasmonic efficiencies of nanoparticles made of metal nitrides (TiN, ZrN) compared with gold, Scientific reports 6 (2016) 38647. https://doi.org/10.1038/srep38647.

[19] W. He, K. Ai, C. Jiang, Y. Li, X. Song, L. Lu, Plasmonic titanium nitride nanoparticles for in vivo photoacoustic tomography imaging and photothermal cancer therapy, Biomaterials 132 (2017) 37–47. https://doi.org/10.1016/j.biomaterials.2017.04.007.

[20] X. Yang, C. Li, L. Yang, Y. Yan, Y. Qian, Reduction-Nitridation Synthesis of Titanium Nitride Nanocrystals, Journal of the American Ceramic Society 86 (2003) 206–208. https://doi.org/10.1111/j.1151-2916.2003.tb03308.x.

[21] H. Zhang, F. Li, Q. Jia, Preparation of titanium nitride ultrafine powders by sol–gel and microwave carbothermal reduction nitridation methods, Ceramics International 35 (2009) 1071–1075. https://doi.org/10.1016/j.ceramint.2008.04.027.

[22] J. Li, L. Gao, J. Sun, Q. Zhang, J. Guo, D. Yan, Synthesis of Nanocrystalline Titanium Nitride Powders by Direct Nitridation of Titanium Oxide, Journal of the American Ceramic Society 84 (2001) 3045–3047. https://doi.org/10.1111/j.1151-2916.2001.tb01136.x.

[23] J. Tavares, S. Coulombe, J.-L. Meunier, Synthesis of cubic-structured monocrystalline titanium nitride nanoparticles by means of a dual plasma process, J. Phys. D: Appl. Phys. 42 (2009) 102001. https://doi.org/10.1088/0022-3727/42/10/102001.

[24] A.A. Popov, G. Tselikov, N. Dumas, C. Berard, K. Metwally, N. Jones, A. Al-Kattan, B. Larrat, D. Braguer, S. Mensah, A. Da Silva, M.-A. Estève, A.V. Kabashin, Laser- synthesized TiN nanoparticles as promising plasmonic alternative for biomedical applications, Scientific reports 9 (2019) 1194. https://doi.org/10.1038/s41598-018-37519-1.

[25] A.V. Kabashin, M. Meunier, Synthesis of colloidal nanoparticles during femtosecond laser ablation of gold in water, J. Appl. Phys. 94 (2003) 7941. https://doi.org/10.1063/1.1626793.

[26] A.V. Kabashin, M. Meunier, Femtosecond laser ablation in aqueous solutions: a novel method to synthesize non-toxic metal colloids with controllable size, J. Phys.: Conf. Ser. 59 (2007) 354–359. https://doi.org/10.1088/1742-6596/59/1/074.

[27] K. Maximova, A. Aristov, M. Sentis, A.V. Kabashin, Size-controllable synthesis of bare gold nanoparticles by femtosecond laser fragmentation in water, Nanotechnology 26 (2015) 65601. https://doi.org/10.1088/0957-4484/26/6/065601.

[28] J.S. Suk, Q. Xu, N. Kim, J. Hanes, L.M. Ensign, PEGylation as a strategy for improving nanoparticle-based drug and gene delivery, Advanced drug delivery reviews 99 (2016) 28–51. https://doi.org/10.1016/j.addr.2015.09.012.

[29] V.M. Petriev, V.K. Tischenko, A.A. Mikhailovskaya, A.A. Popov, G. Tselikov, I. Zelepukin, S.M. Deyev, A.D. Kaprin, S. Ivanov, V.Y. Timoshenko, P.N. Prasad, I.N. Zavestovskaya, A.V. Kabashin, Nuclear nanomedicine using Si nanoparticles as safe and effective carriers of 188Re radionuclide for cancer therapy, Scientific reports 9 (2019) 2017. https://doi.org/10.1038/s41598-018-38474-7.

[30] T.L. Doane, C.-H. Chuang, R.J. Hill, C. Burda, Nanoparticle ζ -potentials, Accounts of chemical research 45 (2012) 317–326. https://doi.org/10.1021/ar200113c.

[31] S. O'Hare, C.K. Atterwill, In Vitro Toxicity Testing Protocols, Humana Press Inc, Totowa, NJ, 1995.

[32] V. Torchilin, Tumor delivery of macromolecular drugs based on the EPR effect, Advanced drug delivery reviews 63 (2011) 131–135. https://doi.org/10.1016/j.addr.2010.03.011.

[33] D. Pan, O. Vargas-Morales, B. Zern, A.C. Anselmo, V. Gupta, M. Zakrewsky, S. Mitragotri, V. Muzykantov, The Effect of Polymeric Nanoparticles on Biocompatibility of Carrier Red Blood Cells, PloS one 11 (2016) e0152074. https://doi.org/10.1371/journal.pone.0152074.

[34] D. Zhang, B. Gökce, S. Barcikowski, Laser Synthesis and Processing of Colloids: Fundamentals and Applications, Chemical reviews 117 (2017) 3990–4103. https://doi.org/10.1021/acs.chemrev.6b00468.

[35] A.H. Hamad, K.S. Khashan, A.A. Hadi, Laser Ablation in Different Environments and Generation of Nanoparticles, in: D. Yang (Ed.), Applications of Laser Ablation - Thin Film Deposition, Nanomaterial Synthesis and Surface Modification, InTech, 2016.

[36] A.-L. Bailly, F. Correard, A. Popov, G. Tselikov, F. Chaspoul, R. Appay, A. Al-Kattan, A.V. Kabashin, D. Braguer, M.-A. Esteve, In vivo evaluation of safety, biodistribution and pharmacokinetics of laser-synthesized gold nanoparticles, Scientific reports 9 (2019) 12890. https://doi.org/10.1038/s41598-019-48748-3.

[37] A. Al-Kattan, Y.V. Ryabchikov, T. Baati, V. Chirvony, J.F. Sánchez-Royo, M. Sentis, D. Braguer, V.Y. Timoshenko, M.-A. Estève, A.V. Kabashin, Ultrapure laser-synthesized Si nanoparticles with variable oxidation states for biomedical applications, Journal of materials chemistry. B 4 (2016) 7852–7858. https://doi.org/10.1039/c6tb02623k.

[38] K.S. Khashan, F.A. Abdulameer, M.S. Jabir, A.A. Hadi, G.M. Sulaiman, Anticancer activity and toxicity of carbon nanoparticles produced by pulsed laser ablation of graphite in water, Mater. Res. Express 11 (2020) 35010. https://doi.org/10.1088/2043-6254/aba1de.

[39] K.S. Khashan, G.M. Sulaiman, S.A. Hussain, T.R. Marzoog, M.S. Jabir, Synthesis, Characterization and Evaluation of Anti-bacterial, Anti-parasitic and Anti-cancer Activities of Aluminum-Doped Zinc Oxide Nanoparticles, J Inorg Organomet Polym 288 (2020) 97. https://doi.org/10.1007/s10904-020-01522-9.

[40] K.S. Khashan, G.M. Sulaiman, R. Mahdi, Preparation of iron oxide nanoparticles-decorated carbon nanotube using laser ablation in liquid and their antimicrobial activity,

Artificial cells, nanomedicine, and biotechnology 45 (2017) 1699–1709. https://doi.org/10.1080/21691401.2017.1282498.

[41] R. Streubel, S. Barcikowski, B. Gökce, Continuous multigram nanoparticle synthesis by high-power, high-repetition-rate ultrafast laser ablation in liquids, Optics letters 41 (2016) 1486–1489. https://doi.org/10.1364/OL.41.001486.

[42] A.R. Rastinehad, H. Anastos, E. Wajswol, J.S. Winoker, J.P. Sfakianos, S.K. Doppalapudi, M.R. Carrick, C.J. Knauer, B. Taouli, S.C. Lewis, A.K. Tewari, J.A. Schwartz, S.E. Canfield, A.K. George, J.L. West, N.J. Halas, Gold nanoshell-localized photothermal ablation of prostate tumors in a clinical pilot device study, Proceedings of the National Academy of Sciences of the United States of America 116 (2019) 18590–18596. https://doi.org/10.1073/pnas.1906929116.

[43] P.M. Gschwend, S. Conti, A. Kaech, C. Maake, S.E. Pratsinis, Silica-Coated TiN Particles for Killing Cancer Cells, ACS applied materials & interfaces 11 (2019) 22550–22560. https://doi.org/10.1021/acsami.9b07239.

[44] S. Jendrzej, B. Gökce, M. Epple, S. Barcikowski, How Size Determines the Value of Gold: Economic Aspects of Wet Chemical and Laser-Based Metal Colloid Synthesis, Chemphyschem a European journal of chemical physics and physical chemistry 18 (2017) 1012–1019. https://doi.org/10.1002/cphc.201601139.

[45] F. Bonaccorso, M. Zerbetto, A.C. Ferrari, V. Amendola, Sorting Nanoparticles by Centrifugal Fields in Clean Media, J. Phys. Chem. C 117 (2013) 13217–13229. https://doi.org/10.1021/jp400599g.

[46] M. Yu, J. Zheng, Clearance Pathways and Tumor Targeting of Imaging Nanoparticles, ACS nano 9 (2015) 6655–6674. https://doi.org/10.1021/acsnano.5b01320.

[47] H.S. Choi, W. Liu, P. Misra, E. Tanaka, J.P. Zimmer, B. Itty Ipe, M.G. Bawendi, J.V. Frangioni, Renal clearance of quantum dots, Nature biotechnology 25 (2007) 1165–1170. https://doi.org/10.1038/nbt1340.

[48] J. Turkevich, G. Garton, P.C. Stevenson, The color of colloidal gold, Journal of Colloid Science 9 (1954) 26–35. https://doi.org/10.1016/0095-8522(54)90070-7.

[49] N. Bertrand, P. Grenier, M. Mahmoudi, E.M. Lima, E.A. Appel, F. Dormont, J.-M. Lim, R. Karnik, R. Langer, O.C. Farokhzad, Mechanistic understanding of in vivo protein corona formation on polymeric nanoparticles and impact on pharmacokinetics, Nature communications 8 (2017) 777. https://doi.org/10.1038/s41467-017-00600-w.

[50] I.V. Zelepukin, A.V. Yaremenko, M.V. Yuryev, A.B. Mirkasymov, I.L. Sokolov, S.M. Deyev, P.I. Nikitin, M.P. Nikitin, Fast processes of nanoparticle blood clearance:

Comprehensive study, Journal of controlled release official journal of the Controlled Release Society 326 (2020) 181–191. https://doi.org/10.1016/j.jconrel.2020.07.014.

[51] N. Bertrand, J. Wu, X. Xu, N. Kamaly, O.C. Farokhzad, Cancer nanotechnology: the impact of passive and active targeting in the era of modern cancer biology, Advanced drug delivery reviews 66 (2014) 2–25. https://doi.org/10.1016/j.addr.2013.11.009.

[52] I.V. Zelepukin, A.V. Yaremenko, V.O. Shipunova, A.V. Babenyshev, I.V. Balalaeva, P.I. Nikitin, S.M. Deyev, M.P. Nikitin, Nanoparticle-based drug delivery via RBC-hitchhiking for the inhibition of lung metastases growth, Nanoscale 11 (2019) 1636–1646. https://doi.org/10.1039/c8nr07730d.

[53] M.P. Nikitin, I.V. Zelepukin, V.O. Shipunova, I.L. Sokolov, S.M. Deyev, P.I. Nikitin, Enhancement of the blood-circulation time and performance of nanomedicines via the forced clearance of erythrocytes, Nature biomedical engineering 4 (2020) 717–731. https://doi.org/10.1038/s41551-020-0581-2.

[54] R. Mohammadinejad, M.A. Moosavi, S. Tavakol, D.Ö. Vardar, A. Hosseini, M. Rahmati, L. Dini, S. Hussain, A. Mandegary, D.J. Klionsky, Necrotic, apoptotic and autophagic cell fates triggered by nanoparticles, Autophagy 15 (2019) 4–33. https://doi.org/10.1080/15548627.2018.1509171.

[55] I.I.J. Alsaedi, Z.J. Taqi, A.M. Abdul Hussien, G.M. Sulaiman, M.S. Jabir, Graphene nanoparticles induces apoptosis in MCF-7 cells through mitochondrial damage and NF-KB pathway, Mater. Res. Express 6 (2019) 95413. https://doi.org/10.1088/2053-1591/ab33af.

[56] H. Kuang, P. Yang, L. Yang, Z.P. Aguilar, H. Xu, Size dependent effect of ZnO nanoparticles on endoplasmic reticulum stress signaling pathway in murine liver, Journal of hazardous materials 317 (2016) 119–126. https://doi.org/10.1016/j.jhazmat.2016.05.063.

[57] H. Hatakeyama, H. Akita, H. Harashima, The polyethyleneglycol dilemma: advantage and disadvantage of PEGylation of liposomes for systemic genes and nucleic acids delivery to tumors, Biological & pharmaceutical bulletin 36 (2013) 892–899. https://doi.org/10.1248/bpb.b13-00059.

[58] E. Fabian, R. Landsiedel, L. Ma-Hock, K. Wiench, W. Wohlleben, B. van Ravenzwaay, Tissue distribution and toxicity of intravenously administered titanium dioxide nanoparticles in rats, Archives of toxicology 82 (2008) 151–157. https://doi.org/10.1007/s00204-007-0253-y.

[59] M. Balazic, J. Kopac, M.J. Jackson, W. Ahmed, Review: titanium and titanium alloy applications in medicine, IJNBM 1 (2007) 3. https://doi.org/10.1504/IJNBM.2007.016517.

[60] F. Correard, K. Maximova, M.-A. Estève, C. Villard, M. Roy, A. Al-Kattan, M. Sentis, M. Gingras, A.V. Kabashin, D. Braguer, Gold nanoparticles prepared by laser ablation in aqueous biocompatible solutions: assessment of safety and biological identity for nanomedicine applications, International Journal of Nanomedicine 9 (2014) 5415–5430. https://doi.org/10.2147/IJN.S65817.

[61] C. Streich, L. Akkari, C. Decker, J. Bormann, C. Rehbock, A. Müller-Schiffmann, F.C. Niemeyer, L. Nagel-Steger, D. Willbold, B. Sacca, C. Korth, T. Schrader, S. Barcikowski, Characterizing the Effect of Multivalent Conjugates Composed of Aβ-Specific Ligands and Metal Nanoparticles on Neurotoxic Fibrillar Aggregation, ACS nano 10 (2016) 7582–7597. https://doi.org/10.1021/acsnano.6b02627.

[62] S. Hebié, Y. Holade, K. Maximova, M. Sentis, P. Delaporte, K.B. Kokoh, T.W. Napporn, A.V. Kabashin, Advanced Electrocatalysts on the Basis of Bare Au Nanomaterials for Biofuel Cell Applications, ACS Catal. 5 (2015) 6489–6496. https://doi.org/10.1021/acscatal.5b01478.

[63] R. Intartaglia, G. Das, K. Bagga, A. Gopalakrishnan, A. Genovese, M. Povia, E. Di Fabrizio, R. Cingolani, A. Diaspro, F. Brandi, Laser synthesis of ligand-free bimetallic nanoparticles for plasmonic applications, Physical chemistry chemical physics PCCP 15 (2013) 3075–3082. https://doi.org/10.1039/c2cp42656k.

[64] M. Kögler, Y.V. Ryabchikov, S. Uusitalo, A. Popov, A. Popov, G. Tselikov, A.-L. Välimaa, A. Al-Kattan, J. Hiltunen, R. Laitinen, P. Neubauer, I. Meglinski, A.V. Kabashin, Bare laser-synthesized Au-based nanoparticles as nondisturbing surface-enhanced Raman scattering probes for bacteria identification, Journal of biophotonics 11 (2018) e201700225. https://doi.org/10.1002/jbio.201700225.

[65] T. Baati, A. Al-Kattan, M.-A. Esteve, L. Njim, Y. Ryabchikov, F. Chaspoul, M. Hammami, M. Sentis, A.V. Kabashin, D. Braguer, Ultrapure laser-synthesized Si-based nanomaterials for biomedical applications: in vivo assessment of safety and biodistribution, Scientific reports 6 (2016). https://doi.org/10.1038/srep25400.

[66] A.Y. Kharin, V.V. Lysenko, A. Rogov, Y.V. Ryabchikov, A. Geloen, I. Tishchenko, O. Marty, P.G. Sennikov, R.A. Kornev, I.N. Zavestovskaya, A.V. Kabashin, V.Y. Timoshenko, Bi‐Modal Nonlinear Optical Contrast from Si Nanoparticles for

Cancer Theranostics, Advanced Optical Materials (2019) 1801728. https://doi.org/10.1002/adom.201801728.

[67] V.A. Oleshchenko, A.Y. Kharin, A.F. Alykova, O.V. Karpukhina, N.V. Karpov, A.A. Popov, V.V. Bezotosnyi, S.M. Klimentov, I.N. Zavestovskaya, A.V. Kabashin, V.Y. Timoshenko, Localized infrared radiation-induced hyperthermia sensitized by laser-ablated silicon nanoparticles for phototherapy applications, Applied Surface Science 516 (2020) 145661. https://doi.org/10.1016/j.apsusc.2020.145661.